Mesoporous silica nanoparticles incorporating squaraine-based photosensitizers: a combined experimental and computational approach

Mesoporous silica nanoparticles incorporating squaraine-based photosensitizers: a combined experimental and computational approach

Ivana Miletto,a Alberto Fraccarollo,a Nadia Barbero,b Claudia Barolo,b Maurizio Cossi,a Leonardo Marchese,a and Enrica Gianottia

Squaraine dyes, that possess intense absorption in the red/near infrared region, have been successfully introduced into mesoporous silica nanoparticles (MSNs) to obtain a nanoplatform for photodynamic therapy. Three brominated squaraine dyes which exhibited good PS performances in solution but different behaviour in vitro due to cell permeability issues, were used as photosensitizer. The effect of the adsorption within the pores of MSNs on the overall UV-Vis-NIR absorption and emission properties as well as on the PS performances was evaluated via a combined experimental and computational physico-chemical approach, which allowed to correlate the unusual optical properties of two out of three system to the dimerization of squaraines on the silica surface, with detrimental effect on the PS performaces. Conversely, the nanoplatform where the squaraine molecules are adsorbed as monomers on the silica surface exhibited the best activity in singlet oxygen generation.

Introduction

Photodynamic therapy (PDT) has emerged in the last decades as an attractive alternative to traditional cancer therapies due to the high selectivity in the destruction of diseased cells over normal cells.1-4 PDT is a photochemistry-based process that uses a light-activatable molecules (the photosensitizer, PS) and light of appropriate wavelength to induce cytotoxicity through the generation of oxidative stress. When the PS is illuminated with light of a specific wavelength, it become activated from a ground state to an excited state. Thanks to its structural features, PS molecules have high tendency to intersystem crossing (ISC), passing form singlet to triplet excited state. As it returns to the ground state, it releases energy, which is transferred to molecular oxygen to generate reactive oxygen species (ROS), such as singlet oxygen ($^1O_2$) and free radicals, that are responsible for the aforementioned oxidative stress and consequent cell death.5,6

The possibility of selectively illuminate the target tissue as well as the short half-life of singlet oxygen7 and other generated ROS, with consequent limited radius of action, together contribute to the high selectivity of PDT.

A suitable PS should exhibit high absorption in the longer wavelength spectral region, ideally in the 600-850 nm region (also known as the photodynamic window, wherein the tissue penetration by light is higher) to minimize interference with endogenous chromophores and yet maintain the energetics necessary for the generation of cytotoxic species such as singlet oxygen. The PS should also exhibit high quantum yield of the triplet state ($\varphi_T>0.4$) and long triplet-state lifetimes ($\tau_T>1$ ms), because the efficiency of the PS is dependent on the photophysical properties of its lowest excited triplet state; furthermore, high photostability is required, along with no or low dark toxicity. It should also be preferentially retained by the diseased target tissue and rapidly excreted from the body.

A wide range of molecules have been proposed as PS, including porphyrins and their precursors, 8 chlorins,9,10 bacteriochlorins, phtalocyanines, xanthene dyes,11 polycyclic heteroaromatic compounds, such us methylene blue etc.12-14 Most of the approved PS are activated by light of wavelength below 600 nm, out of the optimal photodynamic window; as a consequence, in the last years the interest towards to the development of PS absorbing in the red and near-infrared region increased a lot.9,10,15-18 Among the different classes of molecules that can be considered, squaraine dyes attracted intense interest in recent years19; their photophysical properties, i.e. intense absorption in the red/near infrared region, as well as the relative easy tuneable syntheses make squaraine dyes very attractive.

As recently reviewed by Ramaiah et al. 20, the design and development of squaraine dyes as PS has significantly grown in the last twenty years from the time when a squaraine dye was proposed to be a potential candidate, to-date when the use of this class of molecules has been demonstrated in animal models.21 In a recent study by Barbero et al. 22, the synthesis, characterization and photodynamic activity of a series of halogenated symmetric squaraine dyes bearing chains of different lengths on their nitrogen atoms were evaluated. Beside a significant production of singlet oxygen was exhibited in solution by all the molecules tested, different in vitro photodynamic activity was observed. Only squaraine dyes characterized by longer carbon chains on the nitrogen atoms could cause significant reduction in cancer cell growth in vitro. From a SAR (structure-activity relationship) point of view, this behaviour could be related to the fact that longer carbon chains could improve cellular uptake due to the increase of lipophilicity of the overall molecule. It is well known that structural features of PS can strongly influence their effective activity due to solubility issues and permeability through biological membranes, thus limiting the possibility of application of PS in their molecular form.

Over the past decade, nanoparticle-based PDT has emerged as an alternative to conventional PDT to effectively target cancer and to overcome the intrinsic limitations of PS molecules. PS-carrying nanoparticles could increase the water solubility of PS molecules, enhance their permeability through biological barriers and their tumour accumulation, and thus improve the therapeutic efficacy and specificity of PDT. In addition, nanotechnology provides a platform for the integration of multiple functionalities in a single construct.

Various nanomaterials such as liposomes, polymeric nanoparticles, magnetic nanoparticles, quantum dots, carbon-based nanomaterials, mesoporous silica nanoparticles (MSN), as well as several other functional nanoparticles with interesting chemical and physical properties23 have been developed for the delivery of PS, showing encouraging results in vitro and in vivo. Among the various vehicles, MSNs have attracted great interest due to their unique topology that provides MSNs with three distinct domains that can be independently functionalized: the silica framework, the hexagonal pores, and the nanoparticle's outermost surface, thus incorporating the essential capabilities of a theranostic platform in a single particle. In addition to these properties, MSNs have demonstrated high in vivo biocompatibility, straightforward surface functionalization and avid cell uptake.24

In this contribution, a series of three brominated squaraine dyes which exhibited good PS performances in solution but different behaviour in vitro due to cell permeability issues, were physically adsorbed onto MSN. The structural and morphological characterization of the derived nanoplatforms was performed by X-ray powder diffraction (XRPD), High Resolution Transmission Electron Microscopy (HRTEM) and volumetric analysis. The effect of the adsorption within the pores of MSN on the overall UV-Vis absorption and emission properties as well as on the PS performances was evaluated via a combined experimental and computational approach.

The structure of squaraine dyes in DMF solution and physisorbed onto MSNs was also optimized theoretically, with Density Functional Theory (DFT) methods, to understand the structural modifications induced by the adsorption on the silica surface, compared to the conformation of the molecules in solution. The UV-Vis spectra were simulated at the Time Dependent DFT level to support the interpretation of the experimental spectra and again to study the changes due to the physisorption of monomers or dimers on MSN.

Experimental

Materials

Symmetrical indolenine-based squaraine dyes bearing halogenated moieties (Br-NH, Br-C2 and Br-C4, scheme 1) were synthesized as reported elsewhere.22 All other reagents and solvents were purchased by Sigma-Aldrich and used as received unless otherwise specified.

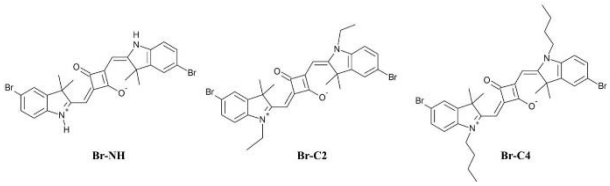

Scheme 1 Chemical structures of the squaraine dyes used for the preparation of the correspondent squaraine/MSN complexes

Synthetic procedures

Preparation of ordered mesoporous silica nanoparticles (MSN). MSN were prepared according to literature procedures using cetyltrimethylammonium bromide (CTAB) as structure directing agents.25,26 CTAB (1 g, 2.74 mmol) was dissolved in 480 ml of distilled water with NaOH (2.0 M, 3.5 ml). The temperature was adjusted at 80°C, then Tetraethyl Orthosilicate (TEOS) (5 ml, 22.4 mmol) was added dropwise under vigorous stirring. The reaction mixture was then stirred at 80°C for 2 h. A white powder precipitated, which was then filtered off and washed with abundant water and methanol, then the CTAB surfactant was removed from the as-prepared material through calcination (at 560°C, under air flux). The ensuing dried MSN were stored as powder.

Preparation of the Br-NH/MSN, Br-C2/MSN and Br-C4/MSN nanoplatforms. MSN aliquots were pre-treated at 100°C overnight and then impregnated with solutions of Br-NH, Br-C2 and Br-C4 in dimethylformamide (DMF). The mixtures were stirred at r.t. overnight, then the solid hybrids were filtered off and dried in air at 100°C. The target squaraine loading performed was 1 wt%; the actual loading of the as-prepared hybrids was evaluated by UV-Vis absorption analysis of the filtered solution. Each sample was washed with fresh DMF, until no free dye was found in the supernatant. Actual loading after washing procedures was then evaluated. Nominal loading and actual loading values after impregnation and after washing are summarized in Table I.

Characterization

X-Ray diffraction (XRD). XRD patterns were obtained by an ARL XTRA48 diffractometer operating with Cu Kα radiation (λ = 1.54062 Å), generated at 40 mA and 40 mV.

Transmission Electron Microscopy (TEM). HRTEM images were collected on a JEOL 3010 High Resolution Transmission Electron Microscope operating at 300 kV. Specimens were prepared by dispersing the sample by sonication in isopropanol and by depositing a few drops of the suspension on carbon-coated grids.

Dynamic Light Scattering (DLS). DLS experiments were performed at 25°C on aqueous MSN (both pure and squaraine-loaded) dispersions using Malvern Zetasizer Nano-ZS Instrument, which uses a 4mW He-Ne laser operating at 633 nm and a detection angle of 173°. Suspensions of 0.05 mg mL-1 of each material were prepared and measured after ultrasonication for 10 minutes.

Volumetric Analysis. N2 physisorption measurements were carried out at 77K in the relative pressure range from 1 x 10-6 to 1 p/p0 by using a Quantachrome Autosorb 1MP/TCD instrument. Prior to the analysis, the samples were outgassed at 373 K for 3 h (residual pressure lower than 10-6 Torr). Specific surface areas were determined using the Brunauer–Emmett–Teller equation, in the relative pressure range from 0.01 to 0.1 p/p0. The desorption branch of the N2 physisorption isotherm was analysed by means of the NLDFT (non-local density functional theory) method, to obtain the pore size distribution of the materials.

Absorption and Diffuse Reflectance UV-Vis spectroscopy. UV-Vis absorption spectra and Diffuse Reflectance (DR) UV-Vis spectra were recorded using a Perkin Elmer Lambda 900 spectrometer equipped with a diffuse reflectance sphere attachment.

Fluorescence. Photoemission and excitation steady state spectra were acquired with a Horiba Scientific Fluorolog spectrofluorimeter equipped with a 450 W Xenon lamp and a Hamamatsu R928 photomultiplier. The spectral response was corrected for the spectral sensitivity of the photomultiplier.

Determination of singlet oxygen generation. 1,3-diphenylisobenzofuran (DPBF) was used as scavenger molecule to evaluate singlet oxygen generation, in fact DPBF rapidly reacts with 1O2 forming the colourless o-dibenzoylbenzene derivative. The 1O2 scavenger activity can be monitored through a decrease in the electronic absorption band of DBPF at 415 nm. A solution of DPBF (20 μM) was added to suspensions of the three different squaraine/MSN nanoplatforms in water and the final suspension was irradiated with a light source at 630 nm (450 W Xenon Lamp). After fixed time intervals, absorption spectra were collected on a Perkin Elmer Lambda 900 instrument. The decrease DBPF absorption contribution at 415 nm was plotted as a function of the irradiation time.

Design of models and computational details. All the calculations were performed with Gaussian09. Ground state equilibrium geometry of the studied squaraine dyes was fully optimized at the DFT level using the B3LYP hybrid functional27 with the Ahlrichs' pVDZ basis set,28 while Hay and Wadt Lanl2dz effective core potentials29,30 and basis set were used to describe the atoms of MSN.

Solvent effects were estimated by the Conductor-like Polarizable Continuum Model (CPCM)31 as implemented in Gaussian09. Dispersion energy corrections were included in all the structure calculations with the semiempirical approach proposed by S. Grimme32 and implemented in Gaussian09 (GD3 procedure). The absorption spectra were simulated with time-dependent (TD)-DFT techniques. Different hybrid and pure functionals were tested for the calculation of absorption spectra. As explained below, LC-ω-PBE showed the best agreement with experimental data and was selected for all the calculations.

Simulated spectra for free squaraine in DMF were computed with long range corrected density functional: LC-ω-PBE.33

The structures of squaraine dyes physisorbed on MSN was also optimized at the DFT level: the silica wall was modelled by a finite cluster (Si) mimicking a hydroxylated amorphous silica surface, based on the same model discussed e.g. in ref. 34. The surface Si/SiO dangling bonds where the silica slab was cut were filled with OH groups.

Results and discussion

Ordered MSN were prepared by a sol-gel synthesis using CTAB as structure directing agent and TEOS as the silica source. The removal of the template was accomplished through calcination of the material at 833 K under air flux. For the preparation of the squaraine/MSN nanoplatforms, aliquots of MSN were pre-treated at 100°C overnight and then they were impregnated with solutions of Br-NH, Br-C2 and Br-C4 for 24h at room temperature. The samples were then recovered by filtration of the reaction mixture and washed until no free dye was found in the washing solution; the so-obtained squaraine/MSNs were addressed to as Br-NH/MSN, Br-C2/MSN and Br-C4/MSN. The target squaraine loading performed was of 1 wt%; such a low loading value was chosen on the basis of previous studies on the loading of luminescent compound into MSNs in which it was demonstrated that at higher loadings the spectroscopic performances can be severely affected by quenching phenomena and inner filter effects.35,36 Actual loading after the washing procedure was evaluated by UV-Vis absorption analysis of the filtered solution and the results are summarized in Table I. In all the three cases, the actual loading was lower than the nominal one, as expected, given the fact that a simple physical adsorption and not a covalent bond was performed. Nevertheless, the final Br-NH/MSN, Br-C2/MSN and Br-C4/MSN samples were found to be stably loaded and no release of squaraine dyes was revealed in water based media, thanks to their limited solubility.

Sample Acronyms	*Nominal loading (wt%)*	*Actual loading* (wt%)	*Actual loading* (mmol/mg)	*Average number of squaraine molecules per NPs*
Br-NH/MSN	1	0.60	1.085·10-5	9578
Br-C2/MSN	1	0.70	1.149·10-5	10147
Br-C4/MSN	1	0.75	1.053·10-5	9296

Table 1 - Squaraine loadings used during the preparation of squaraine/MSN samples (Nominal loading) and after washing procedures (Actual loading)

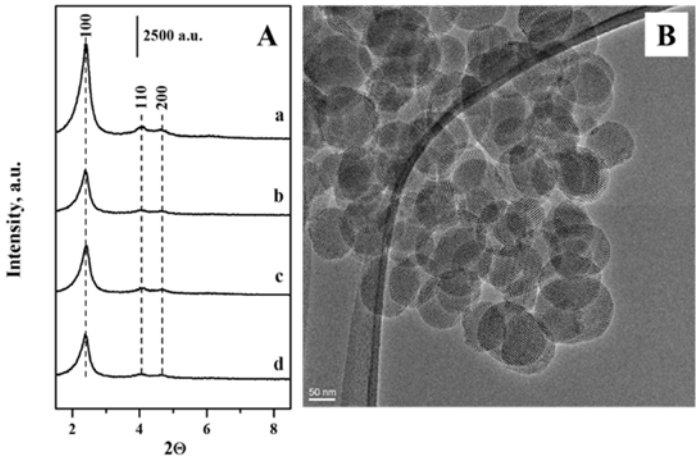

Figure 1 A. XRPD pattern of calcined MCM 41 NPs (a) and squaraine/MSN nanoplatforms: Br-NH/MSN (b); Br-C2/MSN (c) and Br-C4/MSN (d). **B**. Representative HRTEM images of squaraine loaded MSN sample.

In figure 1A the XRPD pattern of calcined MSN and squaraine/MSN nanoplatforms are reported; both the calcined MSN and all the three squaraine loaded systems showed the typical XRPD pattern of an ordered system of channels with hexagonal symmetry, with (100), (110) and (200) reflections. The hexagonal arrangement of the pores, as well as the maintained quasi-spherical morphology, could be observed from the HRTEM images (figure 1B) which revealed the presence of nanostructured nanoparticles with an average diameter of about (150±30 nm), as confirmed by DLS measurements (Table S1).

Volumetric analyses were carried out to evaluate the textural properties of the hybrid materials; N2 adsorption/desorption type IV isotherms with H1-type hysteresis, which are typical of standard M41S materials, were observed both for the calcined MSN and the squaraine/MSN samples. Due to the low squaraine loading performed, no significant variations of Specific Surface Area (ca. 1000 m2g-1) and mean pore diameter (ca. 3.4 nm) were found among the different samples.

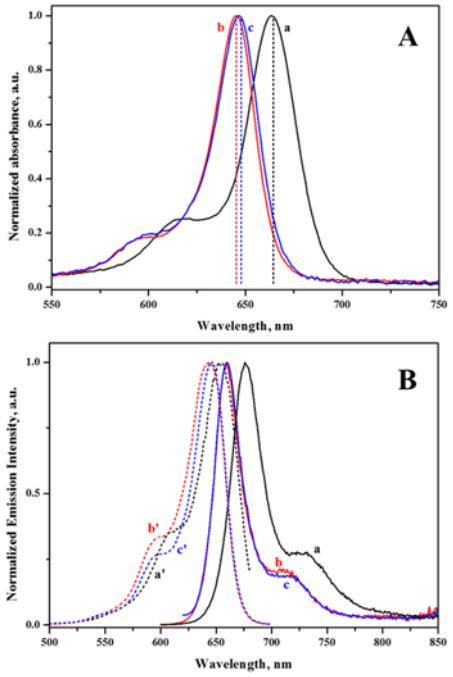

Figure 2 A. Experimental (solid line) and simulated (dotted vertical lines) absorption spectra of Br-NH (black, curve a), Br-C2 (red, curve b) and Br-C4 (blue, curve c) in DMF solution. **B.** Emission (solid lines) and excitation (dashed lines) spectra of Br-NH (black, a, a'), Br-C2 (red, b, b') and Br-C4 (blue, c, c').

To have a better insight into the distribution and dispersion of the squaraine dyes in the different environment of MSNs and hence to correlate the molecular distribution of the fluorophore with the overall performances of the nanomaterials, DR UV-Vis and photoluminescence spectra were recorded and compared to absorption and photoluminescence spectra of squaraine dyes in solution. The same spectra were simulated with TD-DFT calculations: several functionals were tested and, as shown in the ESI (figure S1), the best agreement was obtained with LC-ω-PBE.

Experimental and simulated absorption spectra of Br-NH, Br-C2 and Br-C4 in DMF solution are reported in figure 2A. All the three molecules are characterized by intense absorption band in the 500-700 nm range which exhibits the typical partially resolved vibronic progression,37 with a main contribution centred at 663 nm in the case of Br-NH and at 645 and 647 nm in the case of Br-C2 and Br-C4, respectively, and a hypsochromic shoulder located at 616 nm (Br-NH), 597 nm (Br-C2) and 598 nm (Br-C4). Simulated absorption spectra are in good agreement with the experimental ones (vide infra). As shown in figure 2B, excitation spectra appeared almost coincident with the absorption profiles and the corresponding fluorescence spectra are characterized by a small Stokes shift (ca. 13 nm), as typically exhibited by indole-based squaraine dyes,37,38 and a less pronounced vibronic progression.

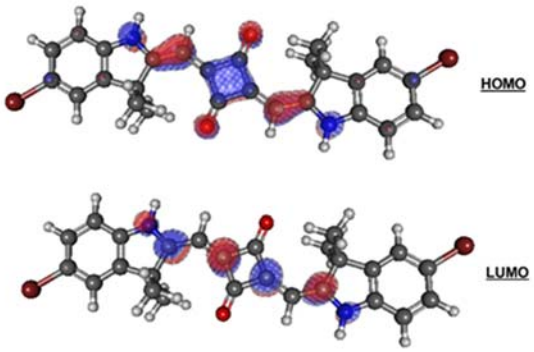

Figure 3 Optimized structure (with HOMO-LUMO orbitals evidenced) of Br-NH molecule in DMF solution

In table 2 the molar extinction coefficient, the absorption maxima with their theoretical estimation, as well as fluorescence maxima and Stokes shift values are reported. Notably, the level of calculation adopted has allowed an almost perfect agreement with the experimental results. In Figure 3 we reported shapes of the HOMO, LUMO orbitals involved in the electronic transitions in Br-NH; the optimized structures of Br-C2 and Br-C4 are reported in the ESI (figure S2).

Table 2 Molar absorption coefficients, maxima wavelength of absorption (experimental and calculated) and emission (experimental) and Stokes shift values of the Br-NH, Br-C2 and Br-C4 molecules in DMF solutions.

Squaraine dye	*Molar absorption coefficient ($M^{-1}cm^{-1}$)*	*Experimental Absorption maxima (nm)*	*Calculated Absorption maxima (nm)*	*Experimental Emission maxima (nm)*	*Stokes Shift (nm)*
Br-NH	215000	663	663	675	12
Br-C2	210000	645	645	659	14
Br-C4	209000	647	647	660	13

The structure of the three squaraine dyes physisorbed onto the silica surface was optimized with the same level of calculation used for the squaraine dyes in vacuum and in DMF solution. In all the adsorbed models the squaraine dyes are quite distorted due to dispersion interactions driving the molecules towards the surface and, to a lesser extent, to hydrogen bond interactions with the silica hydroxyl groups (ESI, figure S3).

As shown in figure 4, in the case of the Br-NH/MSN a good agreement was found between the experimental DR UV-Vis spectra and the calculated absorption values. Upon interaction with the silica surface, a blue shift (ca. 24 nm) of the absorption spectrum was predicted with respect to the absorption spectra of Br-NH in DMF solution, being the calculated absorption maximum of Br-NH/MSN at 639 nm (red, dotted vertical line in figure 4A). The experimental DR UV-Vis spectrum (curve a, figure 4A) is characterized by a maximum at a 642 nm and a bathochromic shoulder at about 730 nm, which can be ascribed to the formation of J-aggregates.39,40 By considering the main absorption band, a blue shift of ca. 21 nm can be calculated with respect to the corresponding spectrum in DMF solution (curve a', figure 4A), which is well in agreement with the calculated one. Similar blue shift can be evidenced in the emission and excitation spectra; the emission spectrum, reported in figure 4B, showed the expected vibronic progression with an emission maximum at 653 nm and a bathochromic shoulder at about 710 nm (675 nm and 730 nm respectively in DMF solution, cfr. figure 2B). The additional large signal detected at longer wavelength (ca.

830 nm) can be correlated to the absorption feature at 730 nm and ascribed to a fraction of squaraine molecules present in the hybrid in form of luminescent aggregates, typically J-aggregates. A confirmation of the nature of the absorption component at ca. 730 nm and its correlation to the emission at 830 nm came from the comparison of the DR UV-Vis and emission spectra of the as-prepared and washed Br-NH/MSN samples (see figure S4).

In the case of both Br-C2/MSN and Br-C4/MSN the agreement was not found between the experimental DR UV-Vis spectra and the simulated absorption bands. On the basis of the simulation, a small red shift was expected for Br-C2 and Br-C4 upon adsorption on silica.

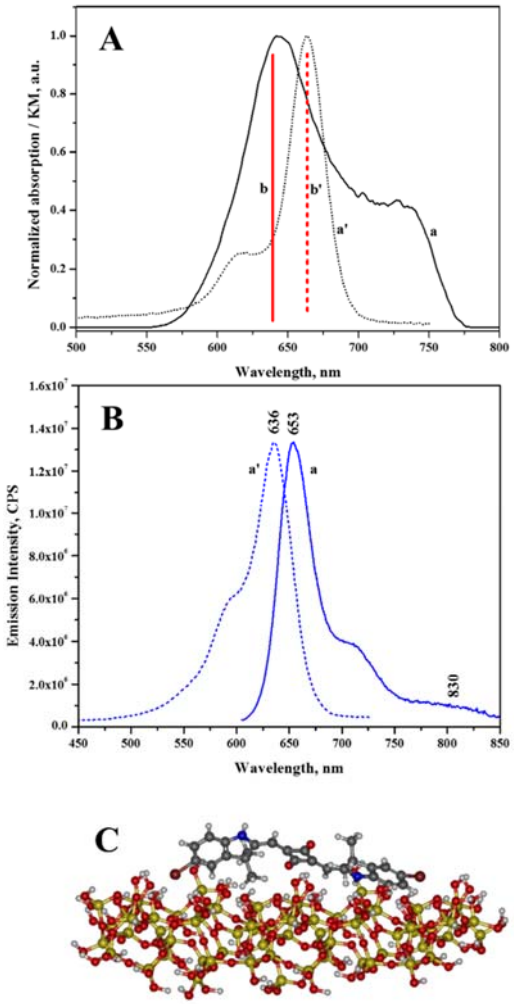

Figure 4 A. Experimental DR-UV-Vis spectrum of Br-NH/MSN (a), UV-Vis absorption spectrum of Br-NH in DMF (a') and simulated absorption energies of Br-NH in DMF solution (b') and physisorbed on silica (b). **B.** Emission (a, solid curve) and excitation (a', dashed curve) spectra of Br-NH/MSN. Emission spectra were obtained upon excitation at 590 nm; excitation spectra were obtained by measuring emission at 700 nm). **C.** Optimized structure of Br-NH physisorbed onto silica surface of MSN.

Conversely, as shown in figure 5, the DR UV-Vis spectra of the Br-C2/MSN and Br-C4/MSN nanoplatforms displayed a more complex absorption pattern, which significantly differed from the simulation. DR UV-Vis spectrum of Br-C2/MSN (figure 5A) is dominated by a component centred at 550 nm and additional less intense bands are present at longer wavelength (615 nm, 676 nm, 698 nm, 800 nm), suggesting a non-uniform distribution of squaraine molecules within the channels of MSN. The more intense component is

significantly blue-shifted (ca. 100 nm) with respect both to the Br-C2 molecule in DMF solution and to what expected for the monomer adsorbed on the silica surface. DR UV-Vis spectrum of Br-C4/MSN (figure 5B) presented an intense band at 557 nm (ca. 90-95 nm blue-shifted both with respect to the spectrum of the monomer in solution and to the simulated spectrum of the dye adsorbed on silica) as well as a signal at 642 nm, in agreement with the simulated absorption of the Br-C4 molecule adsorbed on the silica surface as a monomer. Therefore, it can be concluded that at least a fraction of Br-C4 molecules are present as monomers on the surface of MSN.

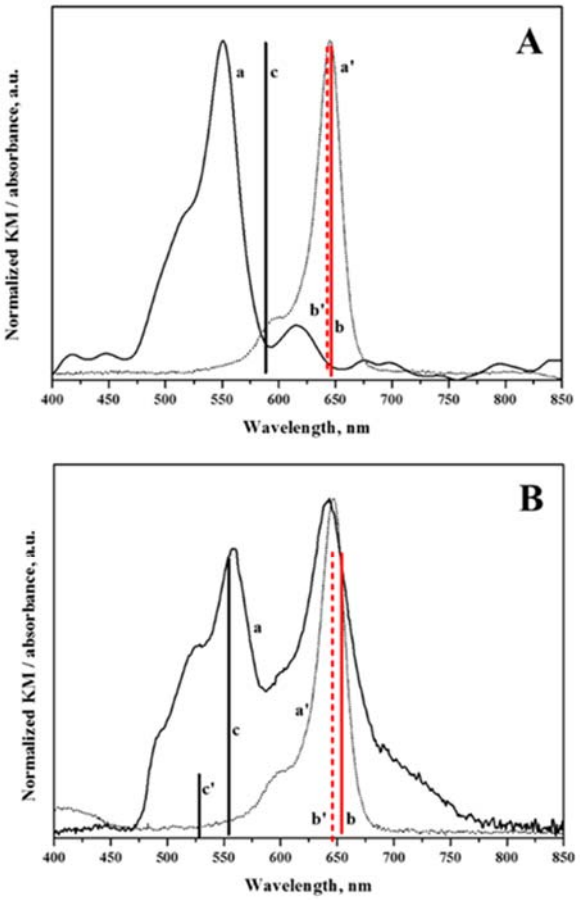

Figure 5. A. DR-UV-Vis spectra of Br-C2/MSN (a, black solid curve), absorption spectrum of Br-C2 in DMF (a', black dotted curve) and simulated absorption of Br-C2/MSN (b, red solid vertical line) and in DMF solution (b', red dashed vertical line). Simulated absorption of Br-C2/MSN dimers on silica surface (c, black solid vertical line). **B.** DR-UV-Vis spectra of Br-C4/MSN (a, black solid curve), absorption spectrum of Br-C4 in DMF (a', black dotted curve) and simulated absorption of Br-C4/MSN (b, red solid vertical line) and in DMF solution (b', red dashed vertical line). Simulated absorption of Br-C4/MSN dimers on silica surface (c, black solid vertical line).

Blue shift in the electronic spectra are usually associated with aggregation phenomena; in particular, there is a relationship between chromophore arrangement and spectral shift, based on the molecular exciton theory. According to exciton theory, the dye molecule is regarded as a point dipole and the excitonic state of the dye aggregate splits into two levels through the interaction of transition dipoles. Dye molecules may aggregate in a parallel way (plane to plane or side by side stacking) to form a sandwich type arrangement (H-dimer) or in a head to tail arrangement (end to end stacking) to form J-dimer. A transition to the upper state in parallel transition moments and to lower state in head-to-tail arrangement with perpendicular transition moments leads to hypsochromic (blue) and bathochromic (red) shifts, respectively.

In order to further investigate the origin of the blue-shifted bands observed in Br-C2/MSN and Br-C4/MSN DR UV-Vis spectra, models of squaraine dimers physisorbed on silica have been optimized and the corresponding absorption bands were simulated (black solid lines in figure 5). As it can be seen in figure 6

where the dimers models are depicted, due to the different steric hindrance of the pending groups, Br-C2 molecules are able to stay stacked on the silica surface, whilst in the case of Br-C4 dimer, one molecule is forced to bend outwards. Simulated absorption bands found for the Br-C4 squaraine adsorbed as a dimer on silica surface are in good agreement with the experimental spectrum; in the case of Br-C2/MSN system, lesser agreement was found, suggesting the presence of a more complex molecules distribution.

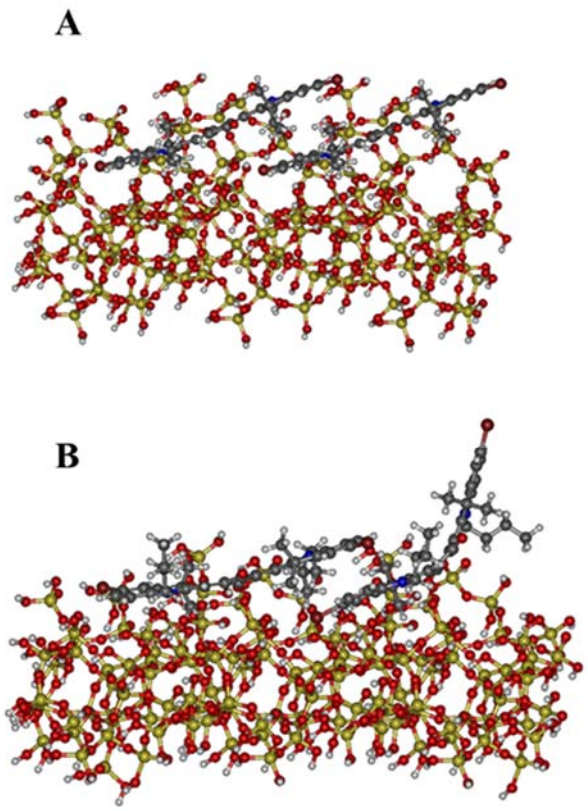

Figure 6. Optimized models Br-C2 (**A**) and Br-C4 (**B**) squaraine molecules adsorbed as dimers on the silica surface

Due to the evident non-uniform distribution of Br-C2 and Br-C4 within the MSN, the analysis of excitation and emission spectra can only provide some qualitative information. Emission and excitation spectra of Br-C2/MSN are reported in figure 7A; the emission spectrum is characterized by a band centred at 635 nm, which position is unchanged irrespectively of the excitation wavelength (λex from 500 nm to 620 nm, data reported in SI, figure S6). The excitation spectrum is similar to the absorption profile, indicating that both absorptions generate the same emission band; in particular, no specific emission seems to be associated with the molecules responsible for the blue-shifted absorption, suggesting that such species are not intrinsically fluorescent but they rather transfer the excitation energy by radiative and/or non-radiative to the luminescent Br-C2 molecules eventually present as monomer in the close proximity. Emission and excitation spectra of Br-C4/MSN, reported in figure 7B, evidenced the presence of an emission band centred at 648 nm with a prominent batochromic shoulder at 690 nm. The broad excitation spectrum is centred around 630 nm and is characterized by the presence of poorly resolved multiple hypsochromic shoulders. Also in this case, the hypsochromic band evidenced in the DR UV-Vis spectrum was not found to generate any specific emission band, as typically reported for non-luminescent aggregates.

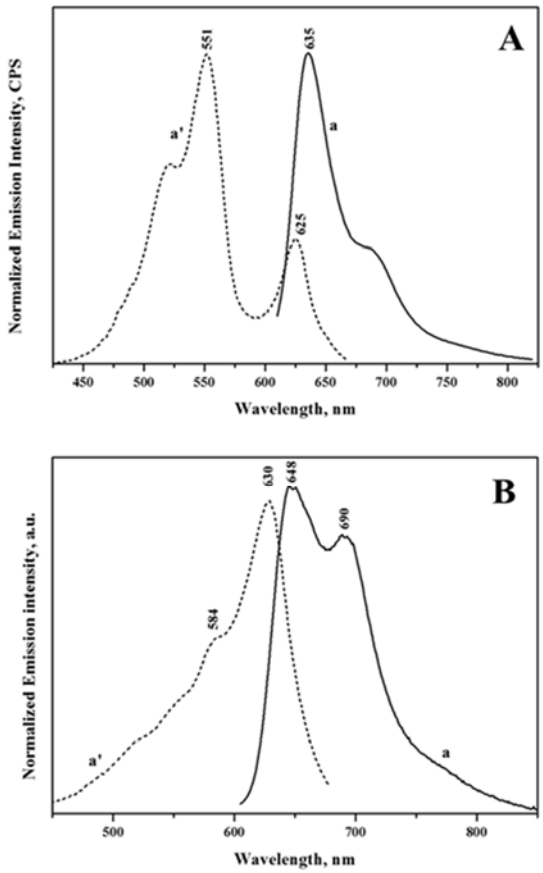

Figure 7. A. Excitation (a', dashed line) and emission spectra (a, solid line) of Br-C2/MSN. **B.** Excitation (a', dashed line) and emission spectra (a', solid line) of Br-C4/MSN

A qualitative and comparative evaluation of the singlet oxygen (1O2) release ability of the three nanoplatforms was carried out by an indirect chemical method, using 1,3-diphenylisobenzofuran (DPBF) as scavenger molecule. DPBF, in fact, rapidly reacts with 1O2 forming the colorless o-dibenzoylbenzene derivative. The 1O2 scavenger activity can be monitored through a decrease in the electronic absorption band of DPBF at 415 nm. The experiments were carried out in aqueous solution irradiated at 630 nm (450 W Xenon Lamp) and the decrease in intensity of the absorption band at 415 nm due to the DBPF oxidation was monitored by UV-Vis absorption spectroscopy for 70 min. The decrease in DBPF absorption at 415 nm was plotted as a function of the irradiation time (figure 8). Irradiation of the MSN sample does not cause an alteration in the DPBF band, as expected, whilst all the squaraine loaded samples possess 1O2 generation ability. In particular, the Br-NH/MSN sample showed the best activity, causing a drop of the DPBF absorption down to the 35%. Br-C2/MSN and Br-C4/MSN samples were found to be less effective in 1O2 release, as an indication that, as usually evidenced in PDT, the aggregation of photosensitizer molecules leads to loss of activity.

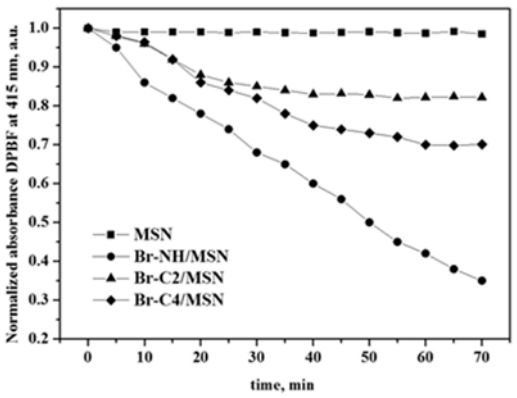

Figure 8. Decrease of the absorption band at 415 nm of DPBF as a function of the irradiation time in presence of MSN and squaraine loaded samples.

Conclusions

In the present study three brominated squaraine dyes which exhibited good PS performances in solution but different behaviour in vitro due to cell permeability issues, were physically adsorbed within MSN. The detailed spectroscopic characterization combined with theoretical calculations, has allowed to have an insight into the effect of the adsorption on silica surface on the optical properties of squaraine dyes. In particular, the good agreement between experimental and simulated absorption spectra of Br-NH/MSN suggested a homogeneous distribution of Br-NH molecules within MSN. Furthermore, the optimization of squaraine dimers adsorption on silica and the simulation of the corresponding absorption bands allowed the correlation of the blue-shifted UV-Vis absorption of the Br-C2/MSN and Br-C4/MSN samples with the presence of squaraine dimers, which are detrimental for the PS activity. Br-NH/MSN nanoplatform, in fact, exhibited the best activity in singlet oxygen generation.

Conflicts of interest

There are no conflicts to declare

Acknowledgements

The authors thanks the MULTY2HYCAT (EU-Horizin 2020 funded project under grant agreement N. 720783) and PRIN-2010A2FSS9 (MIUR Ministry of Education,University and Research) projects for financial support.

References

1 T. J. Dougherty, C. J. Gomer, B. W. Henderson, G. Jori, D. Kessel, M. Korbelik, J. Moan and Q. Peng, J. Natl. Cancer Inst., 1998, 90, 889.

2 D. Dolmans, D. Fukumura and R. K. Jain, Nat. Rev. Cancer, 2003, 3, 380.

3 M. K. Kumova, H. A. Collins, M. Balaz, E. Dahlstedt, J. A. Levitt, N. Sergent, K. Suhling, M. Drobizhev, N. S. Makarov, A. Rebane, H. L. Anderson and D. Phillips, Org. Biomol. Chem., 2009, 7, 889.

4 H. Ding, B. D. Sumer, C. W. Kessinger, Y. Dong, G. Huang, D. A. Boothman and J. Gao, J. Controlled Release, 2011, 151, 271.

5 L. B. Josefsen and R. W. Boyle, Theranostics, 2012, 2(9), 91.

6 M. Mitsunaga, M. Ogawa, N. Kosaka, L. T. Rosenblum, P. L. Choyke and H. Kobayashi, Nat. Med., 2011, 17(12), 1685.

7 A. P. Castano, T. N. Demidova and M. R. Hamblin, Photodiagn. Photodyn. Ther., 2004, 1(4), 279.

8 I. Miletto, E. Bottinelli, A. Siviero, D. Fabbri, P. Calza and G. Berlier, J. Nanopart. Res., 2016, 18(8), 227.

9 E. Gianotti, B. M. Estevão, I. Miletto, S. Tonello, F. Reno' and L. Marchese, ChemistrySelect, 2016, 2, 127.

10 J. P. Celli, B. Q. Spring, I. Rizvi, C. L. Evans, K. S. Samkoe, S. Verma, B. W. Pogue and T. Hasan, Chem. Rev., 2010, 110, 2795.

11 E. Gianotti, B. M. Estevão, F. Cucinotta, N. Hioka, M. Rizzi, F. Renò and L. Marchese, Chem. – Eur. J., 2014, 20, 10921.

12 A. B. Ormond and H. S. Freeman, Materials, 2013, 6, 817.

13 T. Zhao, X. Shen, L. Li, Z. Guan, N. Gao and P. Yuan, Nanoscale, 2012, 4, 7712.

14 N. Adarsh, R. R. Avirah and D. Ramaiah, Org. Lett., 2010, 12, 5720; F. Baldassarre, F. Foglietta, V. Vergaro, N. Barbero, A. L. Capodilupo, L. Serpe, S. Visentin, A. Tepore and G. Ciccarella, J. Photochem. Photobiol., B, 2016, 158, 16.

15 P. Zhang, W. Steelant, M. Kumar and M. Scholfield, J. Am. Chem. Soc., 2007, 129, 4526; N. Barbero, S. Visentin and G. Viscardi, J. Photochem. Photobiol., A, 2015, 299, 38.

16 T. S. Hsieh, J. Y. Wu and C. C. Chang, Chemistry, 2014, 20(31), 9709.

17 I. S. Turan, F. P. Cakmak, D. C. Yildirim, R. Cetin-Atalay and E. U. Akkaya, Chem. – Eur. J., 2014, 20, 16088.

18 X. Li, S. Kolemen, J. Yoon and E. U. Akkaya, Adv. Funct. Mater., 2017, 27, 1604053.

19 D. Ramaiah, A. Joy, N. Chandrasekhar, N. V. Eldho, S. Das and M. V. George, Synthesis, 1997, 783.

20 R. R. Avirah, D. T. Jayaram, N. Adarsh and D. Ramaiah, Org. Biomol. Chem., 2012, 10, 911.

21 A. Abraham, D. D. Gayathri, T. R. Cibin and D. Ramaiah, Proc. SPIE-Int. Soc. Opt. Eng., 2010, 7576, 757603.

22 L. Serpe, S. Ellena, N. Barbero, F. Foglietta, F. Prandini, M. P. Gallo, R. Levi, C. Barolo, R. Canaparo and S. Visentin, Eur. J. Med. Chem., 2016, 113, 187; N. Barbero, C. Magistris, J. Park, D. Saccone, P. Quagliotto, R. Buscaino, C. Medana, C. Barolo and G. Viscardi, Org. Lett., 2015, 17(13), 3306.

23 L. Cheng, C. Wang, L. Feng, K. Yang and Z. Liu, Chem. Rev., 2014, 114, 10869.

24 Y. Chen, H. Chen and J. Shi, Adv. Mater., 2013, 25, 3144.

25 D. R. Radu, C.-Y. Lai, K. Jeftinija, E. W. Rowe, S. Jeftinija and V. S.-Y. Lin, J. Am. Chem. Soc., 2004, 126, 13216.

26 I. Miletto, E. Bottinelli, G. Caputo, S. Coluccia and E. Gianotti, Phys. Chem. Chem. Phys., 2012, 14(28), 10015.

27 M. J. Frisch, G. W. Trucks, H. B. Schlegel, G. E. Scuseria, M. A. Robb, J. R. Cheeseman, G. Scalmani, V. Barone, B. Mennucci, G. A. Petersson, H. Nakatsuji, M. Caricato, X. Li, H. P. Hratchian, A. F. Izmaylov, J. Bloino, G. Zheng, J. L. Sonnenberg, M. Hada, M. Ehara, K. Toyota, R. Fukuda, J. Hasegawa, M. Ishida, T. Nakajima, Y. Honda, O. Kitao, H. Nakai, T. Vreven, J. A. Montgomery Jr., J. E. Peralta, F. Ogliaro, M. Bearpark, J. J. Heyd, E. Brothers, K. N. Kudin, V. N. Staroverov, R. Kobayashi, J. Normand, K. Raghavachari, A. Rendell, J. C. Burant, S. S. Iyengar, J. Tomasi, M. Cossi, N. Rega, J. M. Millam, M. Klene, J. E. Knox, J. B. Cross, V. Bakken, C. Adamo, J. Jaramillo, R. Gomperts, R. E. Stratmann, O. Yazyev, A. J. Austin, R. Cammi, C. Pomelli, J. W. Ochterski, R. L. Martin, K. Morokuma, V. G. Zakrzewski, G. A. Voth, P. Salvador, J. J.

Dannenberg, S. Dapprich, A. D. Daniels, Ö. Farkas, J. B. Foresman, J. V. Ortiz, J. Cioslowski and D. J. Fox, Gaussian 09 revision a.1, Gaussian Inc., Wallingford CT, 2009.

28 A. D. Becke, J. Chem. Phys., 1993, 98, 5648.

29 A. Schafer, H. Horn and R. Ahlrichs, J. Chem. Phys., 1992, 97, 2571.

30 P. J. Hay and W. R. Wadt, J. Chem. Phys., 1985, 82, 270.

31 W. R. Wadt and P. J. Hay, J. Chem. Phys., 1985, 82, 284.

32 M. Cossi, N. Rega, G. Scalmani and V. Barone, J. Comput. Chem., 2003, 24, 669.

33 S. Grimme, J. Antony, S. Ehrlich and H. Krieg, J. Chem. Phys., 2010, 132, 154104.

34 O. A. Vydrov, et al., J. Chem. Phys., 2006, 125, 074106.

35 P. Ugliengo, M. Sodupe, F. Musso, I. J. Bush, R. Orlando and R. Dovesi, Adv. Mater., 2008, 20, 4579.

36 E. Gianotti, C. A. Bertolino, C. Benzi, G. Nicotra, G. Caputo, R. Castino, C. Isidoro and S. Coluccia, ACS Appl. Mater. Interfaces, 2009, 1(3), 678.

37 B. M. Estevão, I. Miletto, L. Marchese and E. Gianotti, Phys. Chem. Chem. Phys., 2016, 18, 9042.

38 R. Borrelli, S. Ellena and C. Barolo, Phys. Chem. Chem. Phys., 2014, 16(6), 2390.

39 C. Gude and W. Rettig, J. Phys. Chem. A, 2000, 104, 8050.

40 M. Kasha, Radiat. Res., 1963, 20(1), 55.

41 A. Patnaik, in J-Aggregates, ed. T. Kobayashi, World Scientific, Singapore, 2012, vol. 2, ch.12, pp. 343–346.